

Symmetric and asymmetric modes of the thermohaline circulation

By REZWAN MOHAMMAD* and JOHAN NILSSON, *Department of Meteorology, Stockholm University, SE-106 91 Stockholm, Sweden*

(Manuscript received 7 April 2005; in final form 12 May 2006)

ABSTRACT

On the basis of a zonally averaged two-hemisphere ocean model, this study investigates how the asymmetric thermohaline circulation depends on the equator-to-pole as well as the pole-to-pole density difference. Numerical experiments are conducted with prescribed surface density distributions as well as with mixed boundary conditions. Further, two different representations of the small-scale vertical mixing are considered, viz. constant and stability-dependent vertical diffusivity. The two mixing representations yield the opposite overturning responses when the equator-to-pole density difference is changed, keeping the shape of the surface density field invariant. However, the overturning responses of the two representations are qualitatively similar when the degree of asymmetry of the surface density field is changed, keeping the density difference invariant. This applies essentially when the freshwater forcing is increased for fixed thermal boundary conditions. For a fixed freshwater forcing, on the other hand, an increase of the equator-to-pole temperature difference yields a weaker asymmetric circulation when the stability-dependent diffusivity is employed, whereas the reverse holds true for the constant diffusivity representation. Further, the numerical experiments show that the hysteresis characteristics of the asymmetric thermohaline circulation may be sensitive to the nature of the small-scale vertical mixing.

1. Introduction

The small-scale vertical mixing, energetically sustained by winds and tides, is one of the key factors controlling the meridional overturning strength in the World Ocean (Wunsch and Ferrari, 2004). However, to quantify the importance of the vertical mixing for the driving of the meridional overturning has proved to be a challenging issue, which is still far from fully resolved. One school of thought (e.g. Munk and Wunsch, 1998) argues that the vertical mixing is crucial for the overturning as well as for its attendant heat transport; a contrary view (e.g. Toggweiler and Samuels, 1995) is that the overturning primarily is forced by wind-induced upwelling in the Southern Ocean.

This study focuses on how the nature of the vertical mixing may impact on the overturning dynamics, in particular the equilibrium response of the overturning to changes in the surface boundary conditions. In order to study this issue in its purest and most simple form, all direct effects of wind-forced circulation are deliberately excluded from the present investigation. Thus, the primary aim here is to examine a process of geophysical relevance using a highly idealized representation of the ocean.

It is well established that, in the absence of wind forcing, the vertical diffusivity is a key factor controlling the meridional overturning strength in a single-hemisphere basin. Straightforward scaling arguments suggest that the overturning strength increases with the vertical diffusivity as well as with the equator-to-pole density difference, a relationship which has proved to be consonant with the outcome of many numerical studies (cf. Park and Bryan, 2000). Huang (1999) pointed out that if the energy supply to vertical mixing is taken to be fixed, the vertical diffusivity becomes inversely proportional to the vertical density difference. Under this assumption, the stronger density stratification associated with an enhanced equator-to-pole density difference serves to suppress the vertical diffusivity. A remarkable consequence of this coupling between the diffusivity and the stratification is that the overturning strength will decrease, rather than increase, with increasing equator-to-pole density difference. These somewhat counterintuitive results have recently been investigated using ocean circulation models of varying complexity (Huang, 1999; Nilsson et al., 2003; Otterå et al., 2003; Mohammad and Nilsson, 2004).

While the dynamical implications of stability-dependent diffusivity have been examined for a single-hemispheric basin, it is by no means straightforward to extrapolate these results to the overturning in the real ocean. A main difficulty is that the overturning in the World Ocean is asymmetric with respect to the equator, a feature that cannot be modelled using a

*Corresponding author.
e-mail: Rezwan.Mohammad@misu.su.se
DOI: 10.1111/j.1600-0870.2006.00194.x

single-hemisphere basin. In addition, wind-forced upwelling in the Southern Ocean is likely to exert control on the overturning strength (Toggweiler and Samuels, 1995; Rahmstorf and England, 1997; Klinger et al., 2003).

Before proceeding, it should again be underlined that the symmetric modes of the thermohaline circulation can be described using classical thermocline scaling (Welander, 1986). In this analysis the key quantities are the small-scale vertical mixing κ , the equator-to-pole surface density difference $\Delta\rho$, and the upwelling area A . The analysis yields that the thermocline depth should scale as

$$H \sim A^{1/3} \kappa^{1/3} \Delta\rho^{-1/3}, \quad (1)$$

and the strength of the circulation as

$$\psi \sim A^{2/3} \kappa^{2/3} \Delta\rho^{1/3}. \quad (2)$$

It should be noted that there currently exists no universal physical description of the vertical mixing in the ocean which predicts how κ depends on $\Delta\rho$ (cf. Toole and McDougall, 2001). When specifying κ it is of interest to compare the dynamical effects of two different assumptions of the physical nature of the small-scale vertical mixing: (i) constant diffusivity, as frequently used in ocean-circulation models, and (ii) a parameterization based on the more conservative hypothesis that the rate of energy available for the mixing is constant, viz. a stability-dependent diffusivity.

In the constant-diffusivity case the scaling implies that the relation between the strength of the circulation and the equator-to-pole density difference is $\psi \sim \Delta\rho^{1/3}$. If the mixing energy is taken to be constant, on the other hand, the diffusivity will depend on the vertical density difference according to $\kappa \sim \Delta\rho^{-1}$ (e.g. Huang, 1999; Nilsson and Walin, 2001). This yields the following scaling:

$$H \sim A^{1/3} \Delta\rho^{-2/3}, \quad (3)$$

$$\psi \sim A^{2/3} \Delta\rho^{-1/3}. \quad (4)$$

The response of the circulation thus differs fundamentally for the two parameterizations of the mixing. When the equator-to-pole density difference is taken to increase, the circulation is strengthened in the constant-diffusivity case, whereas it weakens for stability-dependent diffusivity. A stronger freshwater forcing, which creates a salinity field that reduces the density difference due to temperature, will consequently be associated a stronger overturning if the mixing is stability dependent; for a constant diffusivity the opposite holds true, that is, a stronger freshwater forcing will be associated with a weaker overturning (Nilsson and Walin, 2001). These somewhat counterintuitive overturning dynamics have been simulated in a zonally averaged one-hemisphere model by Mohammad and Nilsson (2004).

How does stability-dependent vertical diffusivity affect the dynamics of equatorially asymmetric regimes of overturning? To approach this question it is illuminating to briefly review previous results concerning asymmetric flow dynamics in models

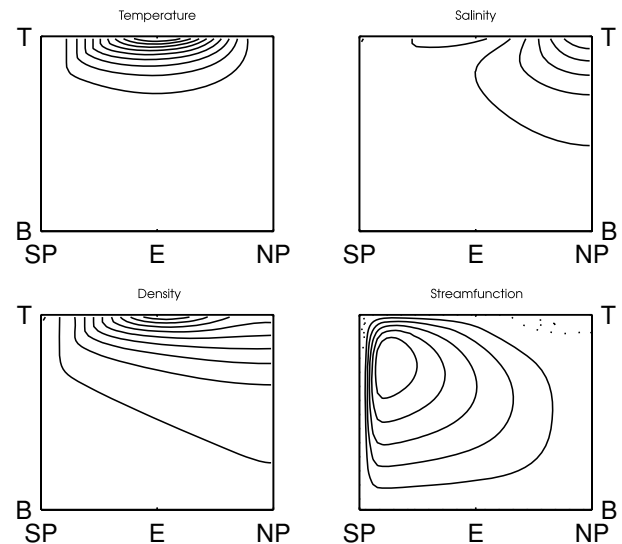


Fig. 1. The structure of the temperature, salinity, density and streamfunction fields for an asymmetric steady-state solution forced by equatorially symmetric mixed boundary conditions, where $R = 0.38$ and constant diffusivity is applied (see Section 4 for details). The isolines are for an arbitrary unit and are the same for the temperature and density fields. The streamfunction of the dominating cell and the subordinate cell is represented with solid lines and dotted lines, respectively. The x -axis is in the meridional direction and the y -axis in the vertical. E is the equator, SP and NP the south and north pole, respectively, T the top and B the bottom.

with constant vertical diffusivity. For the two-hemisphere case, there exists a large number of relevant studies dealing with idealized thermohaline circulation (e.g. Marotzke et al., 1988; Thual and McWilliams, 1992; Vellinga, 1996; Klinger and Marotzke, 1999). Most of these studies have focused on equatorially symmetric mixed boundary conditions, that is, the sea surface temperature is prescribed and the salinity is forced by a surface freshwater flux. For these boundary conditions, the flow dynamics can be summarized as follows. In the presence of no or weak freshwater forcing, the flow is thermally dominated and symmetric with respect to the equator; the downwelling is concentrated towards the poles whereas the upwelling is broadly distributed in the low latitudes. When the freshwater forcing exceeds a critical value, the flow undergoes a subcritical¹ pitchfork bifurcation (Thual and McWilliams, 1992): the symmetric mode becomes unstable and is succeeded by a new asymmetric equilibrium solution. Figure 1 exemplifies this asymmetric state, which is characterized by having stronger sinking in one of the hemispheres (commonly referred to as the dominant hemisphere); in the other (subordinate) hemisphere the sinking is weak or even replaced with upwelling when the freshwater forcing is intense. It should

¹ Dijkstra and Molemaker (1997) have in fact shown that depending on the shape of the freshwater forcing, the bifurcation may either be subcritical or supercritical.

be noted that it is primarily the salinity field that becomes asymmetric, whereas the temperature field remains roughly symmetric (cf. Fig. 1).

The dynamics of the asymmetric flow have been studied in some detail by Klinger and Marotzke (1999), who reported results from a three-dimensional model that employed a constant vertical diffusivity. Based on theoretical considerations and simulations with prescribed surface density, they found that when the degree of asymmetry is fixed the relation between the strength of the overturning and the equator-to-pole density difference in the dominant hemisphere essentially follows the classical one-hemisphere scaling. In this case, the shape of the surface density field is kept invariant. However, they pointed out that the classical scaling is inadequate for describing how the cross-equatorial flow depends on the pole-to-pole density difference when the degree of asymmetry is allowed to change. Further, Klinger and Marotzke (1999) considered the dynamics under mixed boundary conditions. They concluded that, in the dominant hemisphere, the surface equator-to-pole density difference is essentially set by the temperature difference and thus fairly insensitive to the freshwater forcing. In the subordinate hemisphere, on the other hand, the salinity field and thereby the freshwater forcing have a strong influence on the density distribution. Thus, the strength of the main overturning cell is controlled primarily by the equator-to-pole density difference in the dominant hemisphere, whereas the degree of equatorial asymmetry of the flow is set by the pole-to-pole density difference.

The scope of the present study is to extend the previous one-hemisphere analysis due to Mohammad and Nilsson (2004) in order to examine how a stability-dependent vertical diffusivity affects the dynamics of equatorially asymmetric regimes of overturning. In particular, two questions are addressed. The first concerns the relation between the surface density distribution and the asymmetric flow, that is, how the flow depends on the equator-to-pole density difference in the dominant hemisphere as well as the pole-to-pole density difference. A central issue in this context is to what extent the classical one-hemisphere scaling, which predicts a sensitivity to the nature of the vertical mixing, is applicable to the dynamics of the asymmetric flow. The second question is whether a stability-dependent mixing alters the stability and bifurcation properties of the flows that are attained under mixed boundary. Thus, the overarching aim is to determine whether the nature of the vertical mixing may change the dynamics of equatorially asymmetric flows qualitatively.

These questions will be investigated using the simplest possible geometry: a two-hemisphere basin. A zonally averaged model similar to the ones previously employed in various climate studies (Wright and Stocker, 1991; Stocker et al., 1992; Wang and Mysak, 2000) will be employed in the numerical experiments. The presentation is organized as follows. The numerical model is described in Section 2. The outcome of two sets of numerical experiments, the first employing thermal forcing only, and the other with mixed boundary conditions, is reported

in Sections 3 and 4, respectively. In Section 5, the main results are summarized and discussed.

2. The model

The zonally averaged model employed for the present investigation is basically the one previously applied by Mohammad and Nilsson (2004). The main difference is that a two-hemisphere basin now will be used. Essentially, the derivation of the zonally averaged model equations follows Marotzke et al. (1988). The model describes a hydrostatic Boussinesq fluid, confined within a basin of constant depth D , zonal width B , and meridional length $2L$. The closure of the horizontal momentum equation is accomplished by assuming a proportionality between the east-west and north-south pressure gradients, which yields a linear relation between the meridional flow and pressure gradient (see e.g. Wright and Stocker, 1991; Wright et al., 1998).

The following equations govern the system:

$$\gamma v = -\frac{1}{\rho_0} \frac{\partial p}{\partial y}, \quad (5)$$

$$\frac{\partial p}{\partial z} = -\rho g, \quad (6)$$

$$\rho(T, S) = \rho_0(1 - \alpha T + \beta S), \quad (7)$$

$$\frac{\partial v}{\partial y} + \frac{\partial w}{\partial z} = 0, \quad (8)$$

$$\begin{aligned} \frac{\partial}{\partial t} \begin{pmatrix} T \\ S \end{pmatrix} + v \frac{\partial}{\partial y} \begin{pmatrix} T \\ S \end{pmatrix} + w \frac{\partial}{\partial z} \begin{pmatrix} T \\ S \end{pmatrix} \\ = \frac{\partial}{\partial z} \left[\kappa \frac{\partial}{\partial z} \begin{pmatrix} T \\ S \end{pmatrix} \right]. \end{aligned} \quad (9)$$

Here v and w are the zonally averaged meridional and vertical velocities, respectively, γ is a closure parameter relating flow speed and pressure gradient, ρ_0 is the reference density, p is the zonally averaged pressure, y is the meridional coordinate, z is the vertical coordinate, g is the gravity, T and S is the zonally averaged temperature and salinity, respectively, α and β are expansion coefficients for heat and salt, respectively, and κ is the vertical diffusivity.

No transports take place through the solid northern, southern and bottom boundaries. At the surface the salinity is dynamically controlled by a prescribed salinity flux F , given by

$$F(y) = -F_0 \cos\left(y \frac{\pi}{L}\right) = -\kappa \frac{\partial S}{\partial z},$$

where F_0 is the magnitude of the maximum salinity flux. The physical interpretation is that maximal net evaporation and precipitation takes place at the equator and the poles, respectively.

The sea-surface temperature is restored towards the following temperature distribution:

$$T_{\text{top}}(y) = \begin{cases} \frac{\pi T}{2} \{2\mu + (1 - \mu) \times [1 + \cos(y \frac{\pi}{L})]\} & \text{for } y \leq 0, \\ \frac{\pi T}{2} [1 + \cos(y \frac{\pi}{L})] & \text{for } y > 0, \end{cases}$$

where ΔT is the equator-to-pole temperature difference.² The degree of sea-surface temperature asymmetry is represented by a parameter μ , defined as the ratio between the pole-to-pole and the equator-to-pole temperature differences. Note that the sea-surface temperature is restored with a 1 d timescale, implying that the sea-surface temperature is essentially prescribed.

The diffusivity κ is parameterized in two principal ways: as constant (say κ_0) and in such a way that the rate of energy available for mixing (say \mathcal{E}) is constant, implying a stability-dependent diffusivity. Here \mathcal{E} , which equals the rate of increase in potential energy per unit area, is given by (see e.g. Munk and Wunsch, 1998)

$$\mathcal{E}(y) = \rho_0 \int \kappa N^2 dz,$$

where N is the buoyancy frequency. In a stably stratified fluid, a non-zero κ thus leads to the creation of potential energy. Observations as well as theoretical considerations suggest that whereas κ is relatively uniform in the thermocline, it tends to increase towards the bottom, particularly in regions with rough bathymetry (e.g. Toole and McDougall, 2001; Simmons et al., 2004). For the sake of simplicity, we propose two simple vertical distributions of the diffusivity:

Case I: κ is here taken to be vertically uniform over the entire depth, which implies that

$$\mathcal{E}(y) = g\kappa\Delta\rho(y),$$

where $\Delta\rho(y)$ is the vertical density difference between the bottom and the surface. When the diffusivity is stability-dependent $\mathcal{E}(y)$ is taken to be a constant specified by \mathcal{E}_0 . This has the consequence that diffusivity varies horizontally according to

$$\kappa(y) = \frac{\mathcal{E}_0}{g\Delta\rho(y)}. \quad (10)$$

Here we choose \mathcal{E}_0 so that the global production of potential energy, that is, $\int_{-L}^L \mathcal{E}(y) dy$, is the same for both diffusivity representations in a reference state defined below.

Case II: following Gargett (1984) κ is specified as

$$\kappa = a(y)N(y, z)^{-1}. \quad (11)$$

This representation implies that κ tends to increase with depth, reflecting the weaker stratification in the deep ocean. Also in this case, $\mathcal{E}(y)$ is set equal to the constant \mathcal{E}_0 , implying that

$$a(y) = \mathcal{E}_0(\rho_0 \int N dz)^{-1}.$$

Although that these two stability-dependent mixing representations have different spatial distributions κ , they both preserve the global production of potential energy. Thus, the cases I and II are both anticipated to yield one-hemisphere flows that obey the scaling laws (3) and (4).

Note further that for the stability-dependent representations of the mixing, the vertical diffusivity increases with a decreasing stability of the water column. In order to preclude excessive κ -values in areas of weak density stratification, an upper limit is set at $10\kappa_0$. This is to ensure numerical stability. It should be pointed out that observations show that the rate of vertical diffusivity in the ocean varies in space over several orders of magnitude (cf. Toole and McDougall, 2001; Naveira Garabato et al., 2004). In the present simulations, the upper limit on κ tends to be reached in the high latitudes, where the vertical mixing is primarily due to convection. Thus, the limitation on κ is not generally expected to influence our qualitative results. (For the mixing specified by case II, however, the imposed limit may possible distort the dynamics in deep and weakly stratified part of the model.)

We introduce a reference state for which the freshwater forcing is taken to be zero (i.e. $F_0 = 0$) and the flow- and temperature-fields are symmetric (i.e. $\mu = 0$), see Fig. 2. The reference state is characterized by the following parameters: $\Delta T_r = 25^\circ \text{C}$, $\kappa_0 = 10^{-4} \text{ m}^2 \text{ s}^{-1}$, $D = 3000 \text{ m}$, $B = 6000 \text{ km}$, $L = 6000 \text{ km}$, $\alpha = 2 \times 10^{-4} \text{ }^\circ\text{C}^{-1}$, $\beta = 8 \times 10^{-4}$, $\gamma = 1.8 \times 10^{-3} \text{ s}^{-1}$. The thermally induced equator-to-pole density difference, $\Delta\rho_r$, is 5 kg m^{-3} . Note that γ should be regarded as a tuning parameter, here adjusted so that the model yields ocean-like results for the parameter values introduced above. Note furthermore that the reference state will be employed to present the numerical results in non-dimensional form.

In the simulations conducted with mixed boundary conditions, the strength of the freshwater forcing is governed by a non-dimensional parameter R . This quantity is defined as the ratio between the haline buoyancy flux due to the freshwater forcing, and the thermal buoyancy flux associated with the meridional heat transport (say Q_r) in the reference state with zero freshwater forcing. The haline buoyancy flux is $\beta F_0 BL/\pi$, implying that

$$R = \frac{\beta F_0 BL c_p \rho_0}{\alpha Q_r \pi}, \quad (12)$$

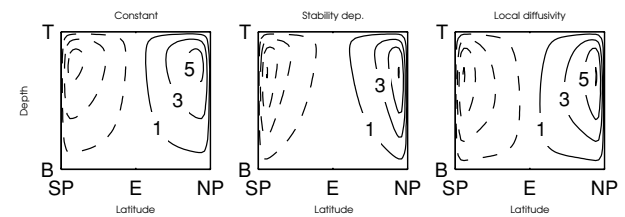


Fig. 2. Reference-state streamfunction for constant diffusivity (left-hand panel) and for the stability-dependent representations case I (middle panel) and case II (right-hand panel). Solid/dashed lines indicate positive/negative values. Note that although the diffusivity differs between the models, they are tuned to have the same rate of potential energy generation in this reference state where $\mu = 0$ and $\Delta T = 25^\circ \text{C}$. The overturning strength is given in Sv.

²The term equator-to-pole difference is here used to denote the difference between equator and the pole harbouring the coldest (or most dense) surface water.

where c_p is the heat capacity of sea water. Note that for constant diffusivity $Q_r = 0.16$ PW and that for the stability-dependent representations $Q_r = 0.11$ PW and $Q_r = 0.09$ PW for case I and case II, respectively. Although the global rate of potential energy generation is the same for the three reference states, the strengths of the heat transport as well as the overturning differs. Thus, the spatial distribution of the diffusivity influences both the amplitude and the structure of the dynamical fields. As seen in Fig. 2, the stability-dependent mixing representations tend to yield a weaker overturning in the low latitudes. This reflects the fact that κ decreases towards the equator in these simulations. For the mixing case II, a general increase of the diffusivity with depth serves to elevate the overturning in the deep ocean; see Cummins et al. (1990) and Nilsson et al. (2003) for a further discussion of how the diffusivity representation where $\kappa \propto N^{-1}$ affects the structure of the overturning.

3. Prescribed surface density

We will now study a thermally forced system without haline effects, that is, $\rho = \rho(T)$. The majority of the results here are non-dimensionalized with respect to the reference state, implying that the reference equator-to-pole temperature difference corresponds to $\Delta T = 1$.

3.1. Fixed degree of asymmetry

In the numerical experiments reported in this section, the ratio between the pole-to-pole and the equator-to-pole temperature differences was held constant ($\mu = 0.5$), that is, the shape of the forcing was retained (cf. Fig. 3). However, the equator-to-pole temperature difference ΔT was varied, and the

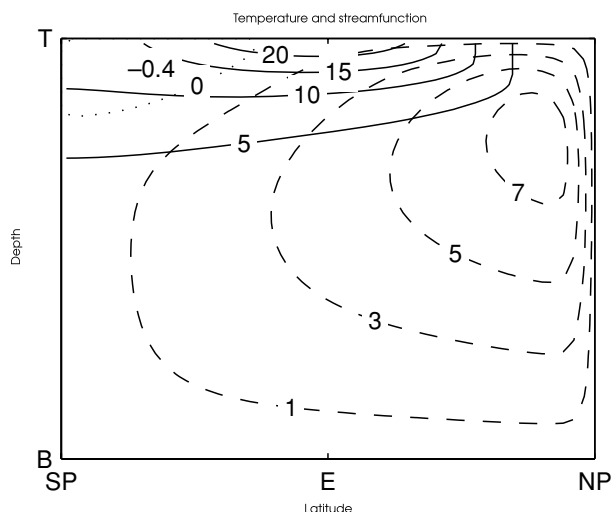


Fig. 3. Steady-state temperature (solid lines) and streamfunction (dashed lines for positive values and dotted for negative) in the basin for $\mu = 0.5$, $\Delta T = 1$ and constant diffusivity. Values given in $^{\circ}\text{C}$ and Sv.

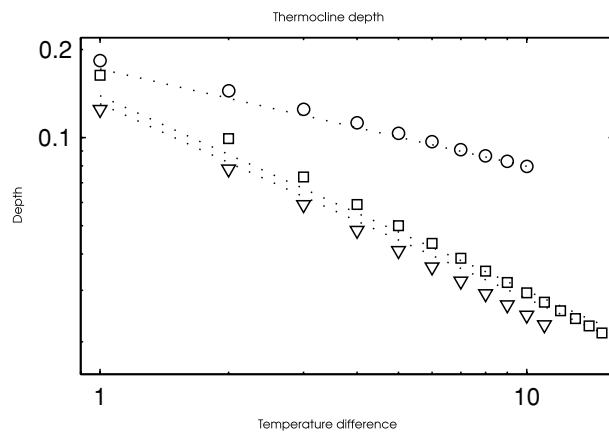


Fig. 4. Thermocline depth index near the center of the southern hemisphere as a function of equator-to-pole temperature difference. The depth index is normalized with the basin depth D , the temperature difference with ΔT_r . Numbers are non-dimensional. Circles, squares and triangles represent results from the numerical model using constant diffusivity and the stability-dependent representations case I and case II, respectively, and dotted lines represent the results from the scale analysis. Axes are logarithmic.

model was integrated to a steady-state solution for each value of ΔT .

Following Mohammad and Nilsson (2004), we introduce a thermocline-depth index that measures the vertical extent of the stratification. This quantity, to be compared with H in the scale analysis, is graphed in Fig. 4 versus the equator-to-pole temperature difference. For both representations of diffusivity, it is seen that the thermocline becomes more shallow with an increasing equator-to-pole temperature difference. The response of the thermocline-depth index is consonant with the predictions of the scale analysis, that is, $H \sim \Delta T^{-1/3}$ and $H \sim \Delta T^{-2/3}$ for constant and stability-dependent diffusivity, respectively.

A broad agreement between theory and numerical simulations is also obtained for the response of the overturning-circulation strength to changes in ΔT , cf. Fig. 5. Here the strength of the overturning is measured by the maximum value of the streamfunction in a column located centrally in the hemisphere where the dominating circulation cell has its maximum, viz. $\max_{z \in [0, D]} [\psi(y \sim 3L/4, z)]$ where z is the vertical coordinate and D is the basin height. Overall, the numerical results approximately follow the scale relations for a one-hemisphere flow: $\psi \sim \Delta T^{1/3}$ and $\psi \sim \Delta T^{-1/3}$ for constant and stability-dependent diffusivity, respectively. For the mixing specified by case II, however, the decrease in overturning with ΔT is weaker than predicted by the scaling law. This discrepancy may be related to the imposed upper limit on κ ; an issue which is not further examined here. Note that although Fig. 5 pertains to the maximum value of the streamfunction over a column in the dominating cell, analogous results are obtained also for the minor circulation cell.

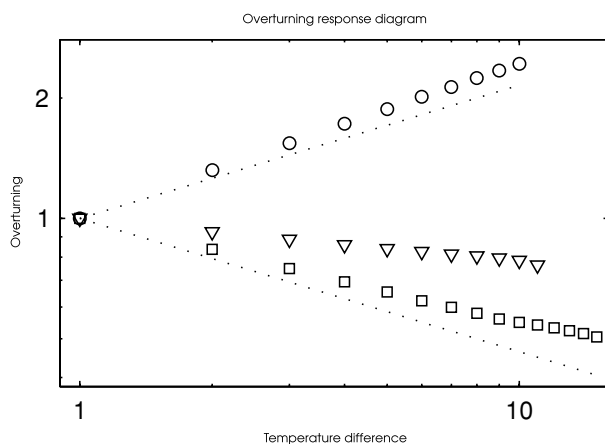


Fig. 5. Overturning response versus the equator-to-pole temperature difference, ΔT . The overturning as well as the temperature difference are non-dimensional and normalized with respect to $\Delta T = \Delta T_r$. Circles, squares and triangles represent results from the numerical model using constant diffusivity and the stability-dependent representations case I and case II, respectively, and dotted lines the scale analysis. Axes are logarithmic.

The correspondence between the two sets of results shows that the scale analysis for symmetric flows also captures the asymmetric mode when μ is kept fixed at 0.5. It is expected that the numerical-model results will follow the scale relations also for other values of μ . It should be underlined that the results shown in Figs. 4 and 5 are representative of the response in the greater part of the basin, the most poleward regions being an exception.

3.2. Varying degree of asymmetry

These numerical experiments were conducted by starting with a reference state where the thermal boundary condition is symmetric ($\mu = 0$ and $\Delta T = 1$) and hereafter increasing μ while holding ΔT fixed. The structural change between the symmetric and asymmetric modes can be described as follows: For symmetric thermal forcing the coldest water is found at the poles. When the pole-to-pole temperature difference, μ , is increased, the coldest surface water is still encountered at the poles in both hemispheres, whereas the warmest deep water is found at the pole in the subordinate hemisphere. Hence the horizontal temperature gradient is reversed below the thermocline. This is illustrated in Fig. 3 (for $\mu = 0.5$) with the isotherm labelled 5°C deepening all the way towards the south pole, implying colder deep water at the equator than at the south pole.

The meridional heat transport, shown in Fig. 6, takes place from the equator towards the poles in the symmetric case. For $\mu = 0.5$ the transport southwards is weak. In the completely asymmetric case the surface heat loss vanishes in the subordinate hemisphere, and the heat transport is directed northwards in the entire basin.

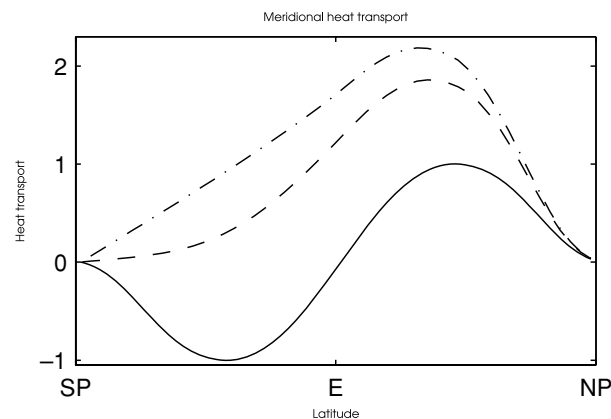


Fig. 6. Meridional (northward) heat transport as a function of the latitude for constant diffusivity. The solid line represents the symmetric case when $\mu = 0$, the dashed line when $\mu = 0.5$ and the dash-dotted line the fully asymmetric case when $\mu = 1$. The heat transport is normalized with the maximum heat transport in the symmetric case.

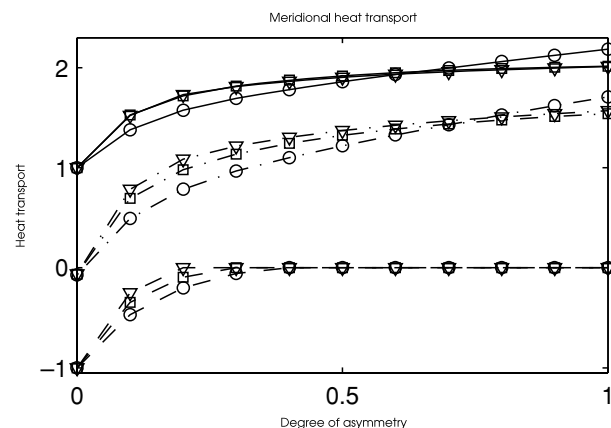


Fig. 7. Meridional (northward) heat transport as a function of the degree of asymmetry for constant (circles) and stability-dependent representations case I (squares) and case II (triangles). The solid and dashed lines show the maximum heat transport in the northern and southern hemisphere, respectively, and the dash-dotted line the heat transport at the equator. The heat transport is normalized with the maximum heat transport in the symmetric case.

Figure 7 shows the meridional heat transport versus the degree of asymmetry. The maximum poleward heat transport in the subordinate hemisphere is seen to decrease quite rapidly as μ grows, and becomes insignificant as μ approaches 0.5. Qualitatively, the present heat-transport responses are similar to that obtained by Klinger and Marotzke (1999), using a three-dimensional model with constant vertical diffusivity.

It should be emphasized that the responses for constant and stability-dependent diffusivities are qualitatively similar to changes in the degree of surface-density asymmetry. A main reason is that changes in the pole-to-pole density difference primarily cause a spatial reorganization of the circulation cells.

This explains why the classical scaling, assuming a constant upwelling area, is insufficient for describing the flow response to changes in the degree of asymmetry of the surface density field.

It can be noted that the decline in strength of the subordinate cell is nearly compensated for by a corresponding increase of the dominating cell. This is visible in Fig. 7, showing that the net poleward heat transport is of the same order in the symmetric and the fully asymmetric cases. Klinger and Marotzke (1999) pointed out that this feature is broadly consistent with the classical scaling if one recognizes that the area of the fully asymmetric cell is roughly twice as large as that of the symmetric one-hemisphere cell; cf. eq. (2). Thus, the flow response to changes in the pole-to-pole density difference is dominated by the changes of the upwelling area of the cells. These changes appear to be qualitatively insensitive to the nature of the vertical mixing.

3.3. Dynamics of asymmetric circulations

As seen above, the horizontal structure of the circulation is considerably modified when the degree of asymmetry of the thermal forcing is varied. Furthermore, the classical one-hemisphere scaling fails to capture the flow response. To illuminate the underlying dynamics, we will discuss the difference between the symmetric and the fully asymmetric case. For the sake of simplicity, we focus initially on a case with constant diffusivity. We start by the following qualitative considerations: For a steady state, the thermodynamic equation (9) is given by

$$v \frac{\partial T}{\partial y} + w \frac{\partial T}{\partial z} = \kappa \frac{\partial^2 T}{\partial z^2}.$$

The equivalent thermal wind equation (5) is

$$\frac{\partial v}{\partial z} = \frac{g\alpha}{\gamma} \frac{\partial T}{\partial y}.$$

Note that the prerequisite for a meridional circulation is that a horizontal temperature gradient be present. In its absence, v must be constant and equal to zero due to mass conservation and hence there will be no meridional circulation.

If we assume that the stratification is controlled by vertical advection and diffusion and that the vertical velocity is independent of depth, the following solution to the thermodynamic equation is obtained:

$$T(y, z) = T_s(y)e^{wz/\kappa}.$$

When $z \rightarrow -\infty$, $T \rightarrow 0$ which implies homogeneous bottom water with no horizontal gradients. Note that consonant with the advective-diffusive balance, the thermocline depth decreases with increasing w . Note furthermore that w , in practice, is a part of the solution and furthermore depends on the depth. However, to view w as independent of z is adequate for the following qualitative discussion:

The meridional derivative of the temperature field is

$$\frac{\partial T}{\partial y} = \left(\frac{\partial T_s}{\partial y} + T_s \frac{z}{\kappa} \frac{\partial w}{\partial y} \right) e^{wz/\kappa}. \quad (13)$$

The two terms $\partial T_s/\partial y$ and $T_s(z/\kappa)(\partial w/\partial y)$, controlling this temperature gradient, may be of different signs and hence counteract one another. In the subordinate hemisphere, an essential difference in the relative importance of these terms is found when comparing the symmetric and the fully asymmetric cases. For $\mu = 0$ there is a significant and dominating surface-temperature gradient, implying that $\partial w/\partial y$ is negligible. For $\mu = 1$ the opposite holds true, since the surface-temperature gradient is non-existent and $\partial w/\partial y$ alone must control the horizontal temperature gradient forcing the circulation.

This qualitative discussion is corroborated by Fig. 8, showing the meridional distribution of the vertical velocity for simulations with constant diffusivity. It is seen that the vertical velocity is more-or-less uniform for $\mu = 0$, and that the latitudinal variations of w are significant for $\mu = 1$. We can also note that even if there is no surface-temperature difference between the equator and the south pole when $\mu = 1$, a meridional overturning circulation is maintained by the meridional density difference below the thermocline (cf. Fig. 3). This feature depends crucially on the meridional variations of the vertical velocity. It should be emphasized that the relation (13) provides a rather poor estimate of the horizontal temperature gradient in the model. Primarily, this is attributable to the depth variation of the vertical velocity and the fact that horizontal advection influences the heat balance. However, the relation (13) tends to correctly predict the sign of the horizontal temperature gradient.

These general results applies also for the stability-dependent mixing specified by case I, where the diffusivity is taken to be independent of the depth but may vary horizontally; cf. eq. (10). In this case, however, the horizontal variations of κ are of importance. Thus, when calculating the relevant form of eq. (13) it is now the horizontal variation of w/κ that matters, rather than the variation of w alone. In fact, for the case I the horizontal distributions of w/κ closely resemble the corresponding ones of w shown in Fig. 8 for a constant diffusivity. In the simulations pertaining to the case II, there is also a tendency that the horizontal variation of w/κ is more pronounced in the subordinate hemisphere of the fully asymmetric flow. However, to analyze the detailed dynamics in this case is more complex due to the vertical variations of κ ; cf. eq. (11).

In conclusion, these considerations suggest that the advective-diffusive balance in combination with the thermal-wind relation essentially govern the stratification for the symmetric as well as the asymmetric flow regimes. For symmetric flows, the density gradient within the thermocline essentially mirrors the surface density gradient. For asymmetric flows, on the other hand, horizontal variations of the vertical velocity (yielding variations in the thermocline depth) are crucial for creating the interior density gradients in the stagnant hemisphere. Thus, it should be possible

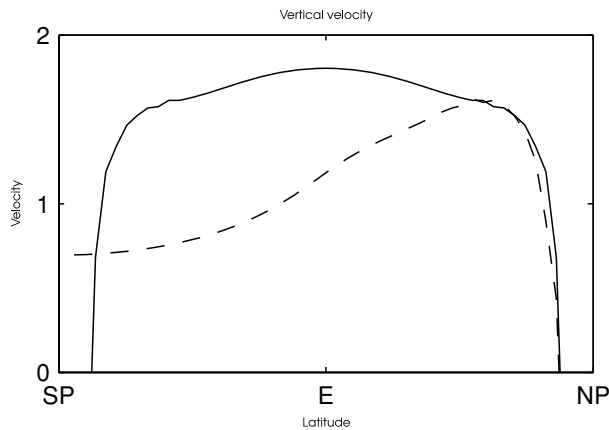


Fig. 8. Vertical velocity as function of latitude at constant depth near the thermocline for the model with constant vertical diffusivity. The solid line pertains to the symmetric case ($\mu = 0$), and the dashed line to the fully asymmetric case ($\mu = 1$). Numbers are given in an arbitrary unit.

to use the physics incorporated in the one-hemisphere scaling to derive a relation for how the upwelling area of the asymmetric overturning cells (i.e. A) depends on the pole-to-pole density difference. We note that Marotzke and Klinger (2000) have made some progress on this issue.

4. Mixed boundary conditions

In this section, the dynamics of thermohaline circulation subjected to mixed boundary conditions will be examined. In all simulations considered here the sea-surface temperature is restored towards the equatorially symmetric temperature profile specified in Section 2. The strength of the freshwater forcing is measured by the non-dimensional parameter R , being essentially the ratio between the haline and thermal buoyancy fluxes; see eq. (12).

Note that no model results calculated for the stability-dependent mixing case II are presented in this section. Some of these solutions, despite long numerical integrations, did not properly converge to a steady state. However, the general results obtained for the case II proved to be qualitatively similar to those pertaining to the case I. For the sake of brevity, we will thus focus on the case I in what follows.

4.1. Varying freshwater forcing

Following Thual and McWilliams (1992) and other previous investigators, we consider the outcome of a suite of numerical calculations where R is gradually increased from zero while keeping the thermal surface forcing constant at $\Delta T = 1$. For each value of R in this suite, the model was integrated until it attained a steady state. As the freshwater forcing is increased, a symmetric salinity distribution develops that reduces the thermally

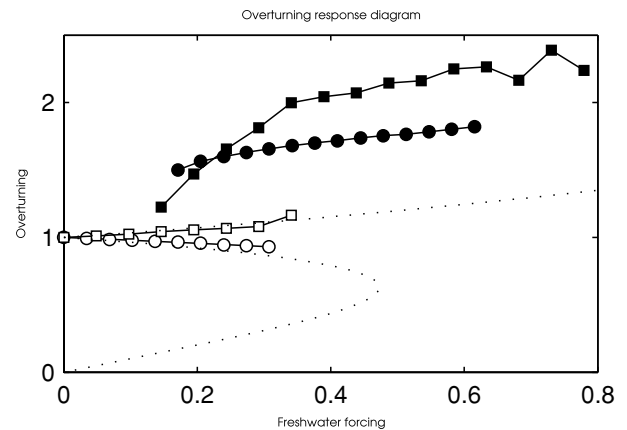


Fig. 9. The overturning strength as function of R . Circles and squares pertain to constant and stability-dependent diffusivity, respectively, and open/filled symbols represent symmetric/asymmetric modes. The overturning is measured by its maximum value in a mid-latitude column located in the hemisphere where the dominating cell has its main abode for the asymmetric modes. Note the overturning strength is presented in non-dimensional form and normalized to be unity when $R = 0$. The dotted lines show theoretical predictions due to Nilsson and Walin (2001). Note further that the asymmetric solutions obtained for the largest values of R , using stability-dependent mixing, exhibited a weak time dependence.

imposed surface density gradient. As illustrated in Fig. 9, the overturning strength becomes weaker when the freshwater forcing is increased in the model with constant diffusivity; the reverse holds true for the model with stability-dependent diffusivity (cf. Mohammad and Nilsson, 2004).

For sufficiently strong freshwater forcing, the symmetric state becomes unstable and is succeeded by a new asymmetric equilibrium; see Fig. 1. This occurs for both types of mixing representations. In the present model, it is a subcritical pitchfork bifurcation that gives rise to the asymmetric flow (cf. Thual and McWilliams, 1992). Note that there are two mirror-image asymmetric equilibrium solutions, which of these states is realized depends on the details of the perturbation destabilizing the symmetric flow. The instability results from an amplification of basin-scale antisymmetric perturbations due to a positive feedback between flow- and salinity-anomalies (e.g. Walin, 1985; Vellinga, 1996; Dijkstra and Molemaker, 1997).

Essentially, the presently simulated transitions from symmetric to asymmetric flow appear to be independent of the nature of the vertical mixing. This behaviour is consistent with the theoretical considerations presented by Nilsson et al. (2004), who argued that the stability of the symmetric equilibrium is primarily controlled by the ratio between the haline and the thermal density differences. Hence, the symmetric flow should become unstable when the ratio $\beta \Delta S / (\alpha \Delta T)$ exceeds a certain threshold, irrespective of how the vertical mixing is parameterized. For the present model the threshold value of $\beta \Delta S / (\alpha \Delta T)$, based on

the surface fields, proved to be about 0.2 for both mixing representations.

We now focus on the response of the asymmetric mode to varying freshwater forcing. The degree of asymmetry of the surface density field grows with the freshwater forcing. Thus, the response of the distribution of density and flow is similar to that examined in Section 3.2, where the asymmetry parameter μ was increased while keeping the equator-to-pole density difference fixed. Figure 9 shows that the freshwater forcing enhances the intensity of the dominant cell, while the subordinate cell simultaneously declines (cf. Klinger and Marotzke, 1999; Wang et al., 1999). Note that this holds true for both representations of the mixing. In a qualitative sense, the flow response appears to be insensitive to the nature of the vertical mixing.

While the response of the asymmetric flow to freshwater forcing is qualitatively similar for the two representations of diffusivity, there are two differences that deserve to be emphasized. First, the degree of asymmetry of the flow is more sensitive to the freshwater forcing when the diffusivity is stability dependent; compare the response of the dominating cell in Fig. 9. This is related to the coupling between the density stratification and the vertical diffusivity, and can be illuminated as follows: In the stagnant hemisphere, where a stable salinity stratification forms, the vertical diffusivity is suppressed. In this region, the surface salinity must thus decrease further to accommodate the diffusive salinity flux dictated by the prescribed surface freshwater forcing. As a consequence, the pole-to-pole density difference and the strength of the dominating cell react more strongly to changes in the freshwater forcing in the model using the stability-dependent diffusivity.

Second, the stability-dependent diffusivity allows for equilibrium solutions, belonging to the asymmetric branch, which only shows a very weak degree of asymmetry; see Fig. 10. This has important consequences for the hysteresis characteristics of the system. Suppose that the flow is in an asymmetric state and that the freshwater forcing is very slowly decreased. For the case with stability-dependent diffusivity, the flow would gradually become less asymmetric, ending with a nearly continuous transition to the branch of symmetric equilibrium solutions. For the case with constant diffusivity, on the other hand, the transition to the symmetric branch would be abrupt and associated with a dramatic reorganization of the flow structure. It should be noted that the transition from the symmetric branch to the asymmetric one is abrupt for both representations of κ .

4.2. Varying thermal forcing

From a climate-change perspective, it is of interest to also examine how the asymmetric mode of thermohaline circulation responds to changes in the thermal boundary conditions for a fixed freshwater forcing. Therefore we have conducted a series of numerical calculations, starting with the asymmetric flows obtained for $R = 0.5$ and $\Delta T = 1$, where steady-state solu-

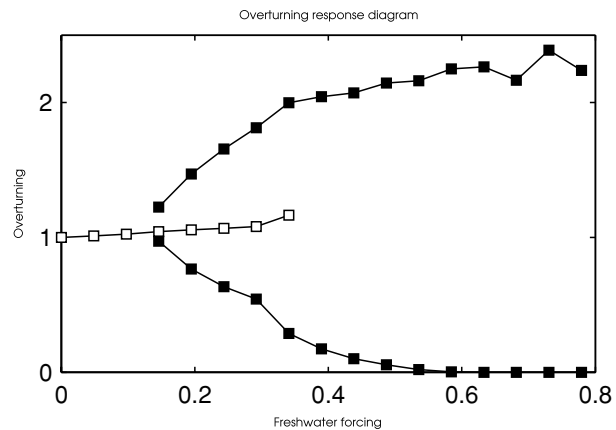


Fig. 10. The overturning strength as function of R for stability-dependent diffusivity. Open/filled symbols represent symmetric/asymmetric modes. For the asymmetric mode, the responses of the dominating and the subordinate cells are shown, measured by the maximum overturning in a mid-latitude column in each hemisphere. Note that the subordinate cell vanishes for stronger freshwater forcing.

tions were calculated for increasing values of ΔT , keeping the freshwater forcing constant. Note that for increasing ΔT , the parameter R decreases; see eq. (12).

The outcome of the numerical calculations can be summarized as follows. When the amplitude of the symmetric surface temperature was enhanced, the degree of asymmetry of the density field weakened, that is, the ratio between the pole-to-pole and equator-to-pole density differences became smaller. This behaviour, primarily related to temperature changes, was identified for both representations of the diffusivity. As shown in Fig. 11,

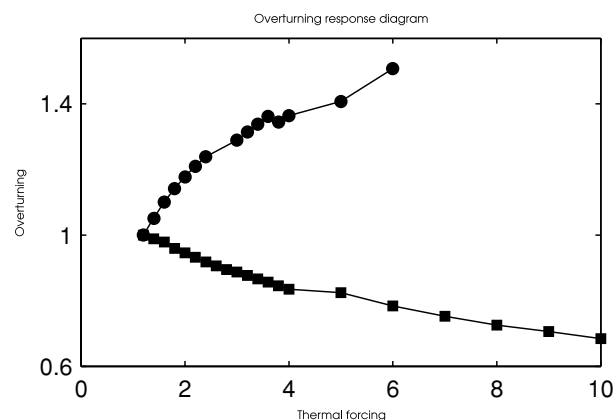


Fig. 11. The response of the dominant cell to changes of ΔT for fixed freshwater forcing. Circles and squares pertain to constant and stability-dependent diffusivity, respectively. The overturning is measured by its maximum value in a mid-latitude column in the hemisphere where the dominating cell has its main abode. The overturning strengths are normalized at $\Delta T = 1$. Note that no asymmetric solutions were obtained for $\Delta T > 6$ when constant diffusivity was employed.

the associated response of the dominating cell to changes in ΔT proved to be more subtle. In the model using stability-dependent diffusivity, the dominant cell becomes weaker when the equator-to-pole difference is enhanced, whereas the opposite holds true in the case of the constant-diffusivity model.

According to the results presented in Section 3, the strength of an asymmetric flow is basically proportional to that of a symmetric flow forced by the same overall density difference; the degree of density asymmetry determines primarily the partitioning between the dominant and the subordinate cell. Thus for a constant freshwater forcing, an increase of ΔT impacts on the strength of the dominant cell in two different ways. To begin with, the associated reduction in the degree of asymmetry tends to decrease the dominant cell. However, the strength of the flow is also affected by the change of overall density contrast, which increases with ΔT . Thus if the vertical diffusivity depends on the stability of the water columns, the dominant as well as the subordinate cell should tend to decline in response to a stronger equator-to-pole temperature difference. For the dominant cell this response serves to reinforce the alterations induced by the reduced degree of asymmetry. Hence when the stability-dependent diffusivity is employed, the strength of the dominant cell should decline when ΔT is increased for a constant freshwater forcing; which indeed can be observed in Fig. 11.

Basically, the reverse applies if the vertical diffusivity is taken to be constant and thus independent of the density stratification. In this case, the overall amplitude of the flow should tend to grow with increasing ΔT . This tendency of the dominant cell to strengthen thus serves to counteract the change caused by the reduction of the density asymmetry. In the present numerical simulations, the enhancement of the equator-to-pole density difference controlled the dominant-cell response, which intensified as ΔT was augmented.

It should further be noted that the model based on stability-dependent mixing yielded asymmetric equilibrium solutions for all the ΔT values in the suite of experiments. When constant diffusivity was employed, the asymmetric solution became unstable when ΔT exceeded 6. For stronger temperature differences, only symmetric steady states were obtained.

5. Discussion

The present study has focused on the dynamics of the asymmetric mode of the thermohaline circulation in a two-hemisphere basin. Using a zonally averaged numerical model, the dependence of the circulation on the equator-to-pole as well as the pole-to-pole density difference has been systematically examined. In summary, the nature of the vertical mixing appears to be crucial for the equilibrium response of the asymmetric thermohaline circulation when changes of the surface boundary conditions lead to alterations of the density difference between the equator and the pole harboring the densest surface water (simply denoted the equator-to-pole density difference here). When the pole-to-pole

density difference is changed, however, the qualitative response of the flow appears to be insensitive to the nature of the vertical mixing.

We believe that the results from the present idealized model may serve to illuminate how the nature of vertical mixing affects the dynamics of a two-hemisphere thermohaline circulation. Thus, our investigation should provide some qualitative information concerning possible impacts of the vertical mixing on the overturning in the real ocean. However, we underline that several geophysically relevant processes and features are absent in the present model. Presumably, the absence of wind forcing and the use of a single basin lacking a periodic 'Southern Ocean' are the most severe idealizations underlying the present study. As demonstrated by Toggweiler and Samuels (1995) as well as Klinger et al. (2003), the impact of wind forcing on the overturning dynamics is significant in ocean basins with circumpolar communication. Furthermore, it would be relevant to examine whether the results from the presently employed zonally averaged model are robust in the sense that they essentially can be reproduced by a three-dimensional general circulation model.

Keeping the idealized nature of the present model in mind, we proceed to speculate on the character of an asymmetric thermohaline circulation in a changed climate. Specifically, we consider a very slow shift of the climatic conditions, which involves an alteration of the surface heat- and freshwater-fluxes. For a single-hemisphere thermohaline circulation, the equilibrium response to such a change will depend crucially on the physics of the vertical mixing, as discussed by e.g. Huang (1999), Nilsson et al. (2003) as well as Mohammad and Nilsson (2004). What do the present results suggest about the response of an asymmetric circulation? Unlike the single-hemisphere case, the details of the changes in the surface forcing appear to decide whether the vertical mixing controls the response of the asymmetric flow. For instance an increase of the freshwater forcing primarily leads to an enhanced pole-to-pole density difference, implying that the dominant cell intensifies irrespective of the features of the vertical mixing. The underlying reason is that the area of the dominant cell expands across the equator into the stagnant hemisphere. Evidently, this structural reorganization has no counterpart in a single-hemisphere basin. It is relevant to note that results from ocean-circulation models reported by Wang et al. (1999) as well as Klinger and Marotzke (1999) also show that a spatially uniform increase in the surface freshwater forcing tends to promote the overturning cell that feeds the dominant deep-water formation site.

It should be noted, however, that a climate change is expected to be associated with alterations of the thermal forcing as well as of the freshwater forcing. Throughout the Earth's history, the meridional gradient of the surface air temperature has varied considerably, being weak during hot-house climate regimes (e.g. the Cretaceous) and strong during glacial climates, cf. Pierrehumbert (2002). The question then is how the hydrological cycle responds when the equator-to-pole temperature difference is altered.

To limit the scope of our discussion, we focus on a warm climate characterized by an equator-to-pole temperature difference that is smaller than that of the present-day climate. Results from atmospheric general circulation models suggest that the atmospheric poleward flux of moisture in the mid-latitudes should slightly increase in a warm low-gradient climate (Pierrehumbert, 2002; Caballero and Langen, 2005). It should be recognized, however, that the moisture flux is affected by two counteracting processes. First, the temperature increase, which permits a higher atmospheric moisture content. Second, the decrease in temperature gradient, which serves to curtail the mid-latitude eddies that carry the moist air poleward. Depending on the details of temperature distribution in the hypothetical warm climate, the moisture flux could thus be stronger as well as weaker than that in the present-day climate (Caballero and Langen, 2005).

For the sake of argument, we assume that the moisture flux is enhanced in our hypothetical warm climate. Assuming further that the energy supply to small-scale mixing is invariant (i.e. stability-dependent diffusivity), we expect to observe the following changes of the asymmetric overturning circulation: To begin with, the combined effect of an increase in freshwater forcing and a decrease in ΔT will enhance the degree of asymmetry of the flow- and density-distributions. Moreover, the decline of the overall oceanic density contrast will be associated with a strengthening of the dominant cell; cf. Section 3.1. Thus the present idealized study suggests that warm climates should be associated with a stronger overturning circulation and hereby a more rapid ventilation of the deep ocean. Evidently, this could have important implications for the biogeochemistry of the ocean. However, the sensitivity of the overturning strength on ΔT is rather weak (see Fig. 11). In fact, the present numerical results indicate that the oceanic heat transport would be diminished in the hypothetical warm climate, despite the overturning strength being enhanced. It deserves to be underlined that the overturning strength as well as the heat transport would decline if the vertical diffusivity instead would have remained constant.

Finally it is worth noting that these considerations bear some relevance for the question whether intense oceanic heat transport could have warmed the poles during past low-gradient climates (e.g. Lyle, 1997; Pierrehumbert, 2002). The present idealized-model results seem to suggest that it is not sufficient to keep the energy supply to small-scale mixing constant in order to drive an enhanced oceanic heat transport in a climate with a reduced equator-to-pole temperature difference. Rather, the rate of energy supply to the small-scale turbulent motion that sustains the vertical mixing presumably needs to be increased. In this context, it is of interest to note that Emanuel (2002) has proposed a mechanism for amplifying the oceanic heat transport in a warm low-gradient climate. Based on thermodynamical considerations, he has showed that the intensity of tropical cyclones should increase in a warmer climate. Thus, the response of the global tropical cyclone activity serves to enhance the wind-driven mixing in

the ocean. Provided that this mixing is sufficiently intense, the oceanic heat transport may be ramped up. Thus, as a concluding comment, the present work serves to illuminate the potential link between warm climatic regimes and alterations of the energy supply to small-scale mixing in the interior of the ocean.

6. Acknowledgments

The work herein reported was undertaken on the basis of a grant from the Swedish National Space Board. We thank professor Peter Lundberg for inspiring discussions and valuable comments.

References

- Caballero, R. and Langen, P. L. 2005. The dynamical range of poleward energy transport in an atmospheric general circulation model. *Geophys. Res. Lett.* **32**, doi:10.1029/2004GL021581.
- Cummins, P. F., Holloway, G. and Gargett, E. 1990. Sensitivity of the GFDL ocean general circulation model to a parameterization of vertical diffusion. *J. Phys. Oceanogr.* **20**, 817–830, doi:10.1175/1520-0485(1990)020<0817:SOTGOG>2.0.CO;2.
- Dijkstra, H. A. and Molemaker, M. J. 1997. Symmetry breaking and overturning oscillations in thermohaline-driven flows. *J. Fluid Mech.* **331**, 169–198, doi:10.1357/002224001762842208.
- Emanuel, K. 2002. A simple model of multiple climate regimes. *J. Geophys. Res.* **107**, doi:10.1029/2001JD001002.
- Gargett, A. E. 1984. Vertical eddy diffusivity in the ocean interior. *J. Mar. Res.* **42**, 359–393.
- Huang, R. X. 1999. Mixing and energetics of the oceanic thermohaline circulation. *J. Phys. Oceanogr.* **29**, 727–746, doi:10.1175/1520-0485(1999)029<0727:MAEOTO>2.0.CO;2.
- Klinger, B. A., Drijfhout, S., Marotzke, J. and Scott, J. R. 2003. Sensitivity of basinwide meridional overturning to diapycnal diffusion and remote wind forcing in an idealized Atlantic-Southern Ocean geometry. *J. Phys. Oceanogr.* **33**, 249–266, doi:10.1175/1520-0485(2003)033<0249:SOBMOT>2.0.CO;2.
- Klinger, B. A. and Marotzke, J. 1999. Behavior of double-hemisphere thermohaline flows in a single basin. *J. Phys. Oceanogr.* **29**, 382–399, doi:10.1175/1520-0485(1999)029<0382:BODHTF>2.0.CO;2.
- Lyle, M. 1997. Could early cenozoic thermohaline circulation have warmed the poles? *Paleoceanography* **12**, 161–167, doi:10.1029/96PA03330.
- Marotzke, J. and Klinger, B. A. 2000. The dynamics of equatorially asymmetric thermohaline circulations. *J. Phys. Oceanogr.* **30**, 955–970, doi:10.1175/1520-0485(2000)030<0955:TDOEAT>2.0.CO;2.
- Marotzke, J., Welander, P. and Willebrand, J. 1988. Instability and multiple steady states in a meridional-plane model of the thermohaline circulation. *Tellus* **40A**, 162–172.
- Mohammad, R. and Nilsson, J. 2004. The role of diapycnal mixing for the equilibrium response of thermohaline circulation. *Ocean Dyn.* **54**, 54–65, doi:10.1007/s10236-003-0065-4.
- Munk, W. H. and Wunsch, C. 1998. Abyssal recipes II: energetics of tidal and wind mixing. *Deep-Sea Res. Part I* **45**, 1977–2010, doi:10.1016/S0967-0637(98)00070-3.
- Naveira Garabato, A. C., Polzin, K. L., King, B. A., Heywood, K. J. and Visbeck, M. 2004. Widespread intense turbulent mixing in the

- Southern Ocean. *Science* **303**, 210–213, doi:10.1126/science.1090929.
- Nilsson, J., Broström, G. and Walin, G. 2003. The thermohaline circulation and vertical mixing: Does weaker density stratification give stronger overturning? *J. Phys. Oceanogr.* **33**, 2781–2795, doi:10.1175/1520-0485(2003)033<2781:TTCAVM>2.0.CO;2.
- Nilsson, J., Broström, G. and Walin, G. 2004. On the spontaneous transition to asymmetric thermohaline circulation. *Tellus* **56A**, 68–78, doi:10.1111/j.1600-0870.2004.00044.x.
- Nilsson, J. and Walin, G. 2001. Freshwater forcing as a booster of thermohaline circulation. *Tellus* **53A**, 629–641, doi:10.1034/j.1600-0870.2001.00263.x.
- Otterå, O. H., Drange, H., Bentsen, M., Kvamstø, N. G. and Jiang, D. 2003. The sensitivity of the present-day atlantic meridional overturning circulation to freshwater forcing. *Geophys. Res. Lett.* **30**, 1898, doi:10.1029/2003GL017578.
- Park, Y.-G. and Bryan, K. 2000. Comparison of thermally driven circulations from a depth-coordinate model and an isopycnal-layer model. Part I: Scaling-law sensitivity to vertical diffusivity. *J. Phys. Oceanogr.* **30**, 590–605, doi:10.1175/1520-0485(2000)030<0590:COTDCF>2.0.CO;2.
- Pierrehumbert, R. T. 2002. The hydrological cycle in deep-time climate problems. *Nature* **419**, 191–198, doi:10.1038/nature01088.
- Rahmstorf, S. and England, M. H. 1997. Influence of southern hemisphere winds on North Atlantic deep water flow. *J. Phys. Oceanogr.* **27**, 2040–2054, doi:10.1175/1520-0485(1997)027<2040:IOSHWO>2.0.CO;2.
- Simmons, H. L., Jayne, S. R., St. Laurent, L. C. and Weaver, A. J. 2004. Tidally driven mixing in a numerical model of the ocean general circulation. *Ocean Model.* **6**, 245–263, doi:10.1016/S1463-5003(03)00011-8.
- Stocker, T. F., Wright, D. G. and Mysak, L. A. 1992. A zonally averaged, coupled ocean-atmosphere model for paleoclimate studies. *J. Climate* **5**, 773–797, doi:10.1175/1520-0442(1992)005<0773:AZACOA>2.0.CO;2.
- Thual, O. and McWilliams, J. C. 1992. The catastrophe structure of thermohaline convection in a two-dimensional fluid model and comparison with low-order box models. *Geophys. Astrophys. Fluid Dyn.*, **64**, 67–95.
- Toggweiler, J. R. and Samuels, B. 1995. Effect of Drake Passage on the global thermohaline circulation. *Deep-Sea Res. Part I* **42**, 477–500, doi:10.1016/0967-0637(95)00012-U.
- Toole, J. M. and McDougall, T. J. 2001. Mixing and stirring in the ocean interior. In: *Ocean Circulation and Climate Volume 77* (eds. G. Siedler, J. Church, and J. Gould), pp. 337–356. Academic Press, Inc.
- Vellinga, M. 1996. Instability of two-dimensional thermohaline circulation. *J. Phys. Oceanogr.* **26**, 305–319, doi:10.1175/1520-0485(1996)026<0305:IOTDTC>2.0.CO;2.
- Walin, G. 1985. The thermohaline circulation and the control of ice ages. *Paleogeogr., Paleoclimatol., Paleoecol.* **50**, 323–332.
- Wang, X., Stone, P. H. and Marotzke, J. 1999. Global thermohaline circulation. Part I: Sensitivity to atmospheric moisture transport. *J. Climate* **12**, 71–82, doi:10.1175/1520-0442(1999)012<0071:GTCPI>2.0.CO;2.
- Wang, Z. and Mysak, L. A. 2000. A simple coupled atmosphere-ocean-sea ice-land surface model for climate and paleoclimate studies. *J. Climate* **13**, 1150–1172, doi:10.1175/1520-0442(2000)013<1150:ASCAOS>2.0.CO;2.
- Welander, P. 1986. Thermohaline effects in the ocean circulation and related simple models. In: *Large-Scale Transport Processes in Oceans and Atmosphere* (eds. J. Willebrand and D. L. T. Anderson) pp. 163–200, D. Reidel Publishing Company.
- Wright, D. G. and Stocker, T. F. 1991. A zonally averaged ocean model for the thermohaline circulation. Part I: Model development and flow dynamics. *J. Phys. Oceanogr.* **21**, 1713–1724, doi:10.1175/1520-0485(1991)021<1713:AZAOMF>2.0.CO;2.
- Wright, D. G., Stocker, T. F. and Mercer, D. 1998. Closures used in zonally averaged ocean models. *J. Phys. Oceanogr.* **28**, 791–804, doi:10.1175/1520-0485(1998)028<0791:CUZAO>2.0.CO;2.
- Wunsch, C. and Ferrari, R. 2004. Vertical mixing, energy and the general circulation of the oceans. *Ann. Rev. Fluid Mech.* **36**, 281–314, doi:10.1146/annurev.fluid.36.050802.122121.